Cell Reports, Volume *23*

Supplemental Information

Conformational Plasticity in Broadly Neutralizing HIV-1 Antibodies Triggers Polyreactivity

Julie Prigent, Annaëlle Jarossay, Cyril Planchais, Caroline Eden, Jérémy Dufloo, Ayrin Kök, Valérie Lorin, Oxana Vratskikh, Thérèse Couderc, Timothée Bruel, Olivier Schwartz, Michael S. Seaman, Oliver Ohlenschläger, Jordan D. Dimitrov, and Hugo Mouquet

SUPPLEMENTAL EXPERIMENTAL PROCEDURES

Recombinant HIV-1 proteins and antibodies

Human anti-gp160 (Buchacher et al., 1994; Burton et al., 1991; Diskin et al., 2013; Diskin et al., 2011; Huang et al., 2012; Mouquet et al., 2012a; Muster et al., 1993; Nelson et al., 2007; Scheid et al., 2011; Trkola et al., 1996; Walker et al., 2011; Walker et al., 2009; Wu et al., 2010; Zhu et al., 2011), ED38 (Meffre et al., 2004) and mGO53 (Wardemann et al., 2003) control antibodies were produced as recombinant monoclonal IgG1 and Fab molecules by co-transfection of FreeStyle™ 293-F cells (Fisher Scientific) using the polyethylenimine (PEI)-precipitation method and purified as previously described (Mouquet et al., 2012a). To generate antibody mutants, single-point mutations were introduced in IgH and IgL genes using directed-site mutagenesis (QuikChange Site-Directed Mutagenesis Kit; Stratagene). To produce trimeric BaL and ZM96 g140 glycoproteins, codon-optimized DNA fragments designed based on the original construct coding for uncleaved YU-2 trimers (Yang et al., 2000) were synthesized and cloned into pcDNA™3.1/Zeo$^{(+)}$ expression vector. YU-2, SS1196 (Mouquet et al., 2012b), BaL, and ZM96 gp140s were produced by transfection of FreeStyle™ 293-F cells using the PEI method (Lorin and Mouquet, 2015) and purified by affinity chromatography using HisPur Cobalt agarose beads (Fisher Scientific) according to the manufacturer's instructions. SF162 gp140 trimers were obtained from the NIH AIDS Reagent Program (#12026).

ELISAs

Polyreactivity ELISAs was performed as previously described (Prigent et al., 2016). Briefly, high-binding 96-well ELISA plates (Costar) were coated overnight with 0.5 µg/well of purified single and double stranded DNA (SD and DD), KLH, LPS, thyroglobulin, lysozyme (Sigma), and 0.25 µg/well of purified insulin (Sigma) in PBS. Purified IgG antibodies were tested at 4 µg/ml and seven consecutive 1:4 dilutions in PBS. For the detection of antibody binding to viral proteins, high-binding 96-well ELISA plates (Costar) were coated overnight with 125 ng/well of purified trimeric HIV-1 gp140 glycoproteins, and recombinant viral envelope

proteins; Chikungunya (CHIKV) p62-E1 (Voss et al., 2010) and hemagglutinin (HA) from influenza B (B/Florida/4/2006, BEI Resources). After blocking and washing steps, purified IgG antibodies in PBS were tested at 16 µg/ml and seven consecutive 1:2 dilutions against HA and p62-E1, and at 4 µg/ml and seven consecutive 1:4 dilutions against HIV-1 gp140 proteins. Control antibodies, mGO53 (negative) (Wardemann et al., 2003), and ED38 (high positive) (Meffre et al., 2004) were included in each experiment. After washings, the plates were revealed by incubation for 1 h with goat HRP-conjugated anti-human IgG antibodies (Immunology Jackson ImmunoReseach, 0.8 µg/ml final), and by adding 100 µl of HRP chromogenic substrate (ABTS solution, Euromedex) after washing steps. Optical densities were measured at 405nm (OD_{405nm}), and background values given by incubation of PBS alone in coated wells were subtracted. Experiments were performed using HydroSpeed™ microplate washer and Sunrise™ microplate absorbance reader (Tecan). HEp-2 ELISAs were performed using the QUANTA Lite™ ANA ELISA Kit (Inova Diagnostics) following the manufacturer's instructions. To determine the ionic strength dependence of the antibody-antigen interactions, ELISAs were performed as described above but with IgG bNAbs at a final concentration of 1.67 or 6.7 nM in 10 mM HEPES pH 7.3 containing different concentrations of NaCl – 0, 5.55, 16.67, 50, 150, 450, and 1350 mM. All ELISA experiments were performed with duplicate or triplicate.

SPR binding assay

All experiments were performed with a Biacore T100 (Biacore, Inc) in HBS-EP+ running buffer (Biacore, Inc) at 25ºC. Purified KLH (Sigma), CHIKV protein p62-E1 (Voss et al., 2010) and human mGO53 IgG (Wardemann et al., 2003) ligands at 250 µg/ml were immobilized on CM5 chips (Biacore, Inc.) by amine coupling at pH 4.5 resulting in an immobilization level of 15,000 RUs. For kinetic measurements on protein-derived chips, IgGs were injected through flow cells at 1 µM in HBS-EP+ running buffer (Biacore, Inc.) at flow rates of 40 µl/min with 3 min association and 5 min dissociation. The sensor surface was regenerated between each experiment with a 30 s injection of 10 mM glycine-HCl pH 2.5 at a flow rate of 50 µl/min.

Sensorgrams were obtained after subtraction of backgrounds (binding to control flow cells and signal of the HBS-EP+ running buffer) using Biacore T100 Evaluation software.

Indirect Immunofluorescence

HIV-1 and control antibodies were analyzed by indirect immunofluorescence on HEp-2 cells (ANA HEp-2, BION Enterprises) and mouse tissues (NOVA Lite® ANA KSL (Mouse Kidney/Stomach/Liver), Inova Diagnostics) sections using FITC-conjugated anti-human IgG antibodies as the tracer according to the manufacturer' instructions. Sections were examined using the fluorescence microscope Axio Imager 2 (Zeiss) with ApoTome.2 system, and pictures were taken at magnification x 40 with 7000 ms-acquisition using ZEN imaging software (Zen 2.0 blue version, Zeiss) at the Imagopole platform (Institut Pasteur).

Western blotting

Protein extracts were prepared from cell pellets of freshly cultivated human laryngeal carcinoma HEp-2 cells (ATCC® CCL-23™) and *E. coli* (DH10b, Life technologies) using RIPA buffer-based extraction method (Cell signaling technology). The final concentration of protein lysates was determined using Bradford reagent assay (Sigma). Proteins (17.5 µg total/well) were separated by SDS-PAGE with a NuPAGE® 4-12% Bis-Tris Gel (Invitrogen), and electrotransferred onto nitrocellulose membranes. The filters were then saturated for 2 h in PBS-0.05% Tween 20 (PBST)-5% dry milk, and incubated with human monoclonal antibodies (at 10, 20 and 30 µg/ml) in PBST-5% dry milk for 2 h. After washing with PBST, filters were incubated for 1 h with 1/25,000-diluted Alexa Fluor 680-conjugated donkey anti-human IgG (Jackson ImmunoReseach) in PBST-5% dry milk. Finally, membranes were washed, and examined with the Odyssey Infrared Imaging system (LI-COR Biosciences).

Flow cytometry binding assay

Virus stocks for YU-2b and transmitted-founder HIV-1 strains (CH058, CH077 and WITO; NIH AIDS Reagent Program) were prepared by the transfection of 293T cells as previously

described (Casartelli et al., 2010). CEM-NKR-CCR5 cells (NIH AIDS Reagent Program) were infected with viral inocula adjusted to achieve 10-30% of Gag^+ cells at 48 h post infection. Infected cells were incubated with IgG antibodies (at 0.1, 1 and 10 µg/ml) for 30 min at 37°C in staining buffer (PBS, 0.5% BSA, 2mM EDTA), washed, and incubated 30 min at 4°C with AF647-conjugated anti-human IgG antibodies (1:400 dilution; Life technologies). Cells were then fixed with 4% paraformaldehyde and stained for intra-cellular Gag as previously described (Bruel et al., 2016). Data were acquired using an Attune Nxt instrument (Life Technologies) and analyzed using FlowJo software (v10.3; FlowJo LLC). In each experiment, the % of binding to Gag^+ and MFI values were calculated and background values given by incubation of IgGs with non-infected cells alone were subtracted. All experiments were performed with triplicate.

CHIKV neutralization assays

To assay for CHIKV neutralization, serially diluted IgG antibodies (at 50 µg/ml and 7 consecutive 1:4 dilutions) were incubated for 1 h at 37°C with recombinant *Renilla* luciferase-expressing CHIKV (Henrik Gad et al., 2012). Mixtures were then added to Vero cell monolayers and following a 1 h incubation at 37°C, supernatants were removed and cells were washed twice with DMEM followed by the addition of 10% FBS DMEM. Six hours later, cells were washed with PBS and lysed (Renilla Luciferase Assay System, Promega). After mixing the substrate (Renilla Luciferase Assay System, Promega) with cell lysates, luciferase activity was measured on the Enspire microplate luminometer (Perkin Elmer). The percent neutralization was calculated using the formula: [1 − (luciferase activity in cells treated with the virus/antibody mixture) / (luciferase activity in cells treated with virus alone)] × 100. Nonlinear regression analyses (using *Richard's 5 parameter dose-response curve* fitting) were performed, and IC50 values were determined using Graph Pad Prism v.6. A neutralization plaque assay was also performed with La Réunion CHIKV-21 isolate (Schuffenecker et al., 2006). The assay was performed in 96-well plates by incubating 50 µl containing 100 TCID50 (tissue-culture infectious dose) of CHIKV-21 with 50 µl of antibody

serially diluted twofold from 20 µg to 0.16 µg. After incubation at 37°C for 1h, 100 µl of Vero cells ($2x10^3$ cells) were added into each well, and plates were maintained at 37°C. After 5 days, the cells were observed to score a cytopathic effect. Neutralization titers corresponded to the highest antibody dilution able to fully protect cells from cytopathic effect. Positive and negative controls for cytopathic effect included wells containing cells with CHIKV without antibody and wells with mock infections, respectively. Anti-CHIKV neutralizing antibody able to completely neutralize viral infectivity at 2.5 µg was used as positive control for the neutralization assay. All experiments were performed with duplicate.

SPR affinity and thermodynamic analyses

To measure the apparent affinity of HIV-1 bNAbs (IgG and Fabs) to KLH, YU-2 and ZM-96 gp140 trimers, CM5 chips (Biacore, Inc.) were immobilized by amine coupling to reach immobilization levels of 9,000 RUs and 300-500 RUs, respectively (Mouquet et al., 2010). IgGs and Fabs at a concentration of 500 nM or 250 nM and 7 successive 1:2 dilutions in HBS-EP+ running buffer (Biacore, Inc.) were injected through flow cells at flow rates of 30 µl/min with 3 min association and 8 min dissociation. The sensor surface was regenerated between each experiment with a 30-60 s injection of 5 M $MgCl_2$. Experiments were performed with a Biacore 2000 (Biacore, Inc), and evaluation of kinetic data was performed using the BIAevaluation software (v4.1.1, Biacore) by applying 1:1 binding Langmuir model.

Thermodynamic parameters were determined using Eyring's analyses as previously described (Hadzhieva et al., 2017). Briefly, kinetic rate constants obtained at distinct temperatures (10, 15, 20, 25, 30, 35°C) were used to build Arrhenius plots. The values of slopes of the Arrhenius plots were calculated by using a linear regression analysis in GraphPad Prism v.6 (GraphPad Prism Inc. USA) and substituting the slopes into the equation Ea = -slope × R, where the "slope" = $\partial \ln(k_{a/d}) / \partial (1/T)$ and Ea is the activation energy. The changes in enthalpy, entropy and Gibbs free, characterizing the association and dissociation phases were estimated by using the equations: $\Delta H^{\ddagger} = Ea - RT$; $\ln(k_{a/d}/T) = -$

$\Delta H^{\ddagger}/RT + \Delta S^{\ddagger}/R + \ln(k'/h)$; $\Delta G^{\ddagger} = \Delta H^{\ddagger} - T\Delta S^{\ddagger}$, where T is the temperature in Kelvin degrees, k′ is the Boltzman constant and h is the Planck's constant. The equilibrium values of the thermodynamic parameters were calculated using the equations: $\Delta G_{eq} = \Delta G^{\ddagger}_{a} - \Delta G^{\ddagger}_{d}$; $\Delta H_{eq} = \Delta H^{\ddagger}_{a} - \Delta H^{\ddagger}_{d}$; $T\Delta S_{eq} = T\Delta S^{\ddagger}_{a} - T\Delta S^{\ddagger}_{d}$. The equilibrium thermodynamic parameters were also calculated by using Van't Hoff equation. Activation and equilibrium thermodynamic parameters were determined at a reference temperature of 25°C (298.7 K).

Molecular dynamics simulation

Molecular dynamics simulations of the antibodies were performed with the AMBER v.12 Molecular Dynamics program suite (D.A. Case, 2012; D.A. Pearlman, 1995; R. Salomon-Ferrer, 2013). Explicit solvent within a rectangular water box was added and the starting structures were energy-minimized by applying the steepest descent and conjugate gradient algorithm for 1000 steps each. During a heating phase, the temperature was gradually adjusted to 300 K. The molecular dynamics (MD) simulations with the program module SANDER were performed for the duration of 2 ns at constant pressure with a time step of 2 fs (using the SHAKE algorithm) and a cut-off of 8 Å. Coordinates were stored every 2 ps. For analysis, data sets were selected every 2 ps. Root-mean-square (rms) values were calculated relative to the first coordinate set of the MD trajectory using the CPPTRAJ module v.13.10. Average rms values specified in the text were calculated for the 2^{nd} ns of the trajectory. As the IgH loop 101-114 in the available m66 structure was disordered, it was excluded from the rms analyses, which were run on residues 1-100 and 115-130 of IgH and 1-107 of IgL. Trajectories were visualized and figures were produced with VMD (Humphrey et al., 1996).

SUPPLEMENTAL REFERENCES

Buchacher, A., Predl, R., Strutzenberger, K., Steinfellner, W., Trkola, A., Purtscher, M., Gruber, G., Tauer, C., Steindl, F., Jungbauer, A*., et al.* (1994). Generation of human monoclonal antibodies against HIV-1 proteins; electrofusion and Epstein-Barr virus transformation for peripheral blood lymphocyte immortalization. AIDS research and human retroviruses *10*, 359-369.

Burton, D.R., Barbas, C.F., 3rd, Persson, M.A., Koenig, S., Chanock, R.M., and Lerner, R.A. (1991). A large array of human monoclonal antibodies to type 1 human immunodeficiency virus from combinatorial libraries of asymptomatic seropositive individuals. Proceedings of the National Academy of Sciences of the United States of America *88*, 10134-10137.

Casartelli, N., Sourisseau, M., Feldmann, J., Guivel-Benhassine, F., Mallet, A., Marcelin, A.G., Guatelli, J., and Schwartz, O. (2010). Tetherin restricts productive HIV-1 cell-to-cell transmission. PLoS pathogens *6*, e1000955.

D.A. Case, T.A.D., T.E. Cheatham, III, C.L. Simmerling, J. Wang, R.E. Duke, R. Luo, R.C. Walker, W. Zhang, K.M. Merz, B. Roberts, S. Hayik, A. Roitberg, G. Seabra, J. Swails, A.W. Götz, I. Kolossváry, K.F. Wong, F. Paesani, J. Vanicek, R.M. Wolf, J. Liu, X. Wu, S.R. Brozell, T. Steinbrecher, H. Gohlke, Q. Cai, X. Ye, J. Wang, M.-J. Hsieh, G. Cui, D.R. Roe, D.H. Mathews, M.G. Seetin, R. Salomon-Ferrer, C. Sagui, V. Babin, T. Luchko, S. Gusarov, A. Kovalenko, and P.A. Kollman (2012). AMBER 12. University of California, San Francisco.

D.A. Pearlman, D.A.C., J.W. Caldwell, W.S. Ross, T.E. Cheatham, III, S. DeBolt, D. Ferguson, G. Seibel, and P. Kollman (1995). AMBER, a package of computer programs for applying molecular mechanics, normal mode analysis, molecular dynamics and free energy calculations to simulate the structural and energetic properties of molecules. Comp Phys Commun *91*, 1-41.

Henrik Gad, H., Paulous, S., Belarbi, E., Diancourt, L., Drosten, C., Kummerer, B.M., Plate, A.E., Caro, V., and Despres, P. (2012). The E2-E166K substitution restores Chikungunya virus growth in OAS3 expressing cells by acting on viral entry. Virology *434*, 27-37.

Huang, J., Ofek, G., Laub, L., Louder, M.K., Doria-Rose, N.A., Longo, N.S., Imamichi, H., Bailer, R.T., Chakrabarti, B., Sharma, S.K*., et al.* (2012). Broad and potent neutralization of HIV-1 by a gp41-specific human antibody. Nature *491*, 406-412.

Humphrey, W., Dalke, A., and Schulten, K. (1996). VMD: visual molecular dynamics. Journal of molecular graphics *14*, 33-38, 27-38.

Meffre, E., Schaefer, A., Wardemann, H., Wilson, P., Davis, E., and Nussenzweig, M.C. (2004). Surrogate light chain expressing human peripheral B cells produce self-reactive antibodies. J Exp Med *199*, 145-150.

Muster, T., Steindl, F., Purtscher, M., Trkola, A., Klima, A., Himmler, G., Ruker, F., and Katinger, H. (1993). A conserved neutralizing epitope on gp41 of human immunodeficiency virus type 1. J Virol *67*, 6642-6647.

Nelson, J.D., Brunel, F.M., Jensen, R., Crooks, E.T., Cardoso, R.M., Wang, M., Hessell, A., Wilson, I.A., Binley, J.M., Dawson, P.E*., et al.* (2007). An affinity-enhanced neutralizing antibody against the membrane-proximal external region of human immunodeficiency virus type 1 gp41 recognizes an epitope between those of 2F5 and 4E10. J Virol *81*, 4033-4043.

R. Salomon-Ferrer, D.A.C., and R.C. Walker. (2013). An overview of the Amber Biomolecular Simulation Package. WIREs Comput Mol Sci *3*, 198-210.

Schuffenecker, I., Iteman, I., Michault, A., Murri, S., Frangeul, L., Vaney, M.C., Lavenir, R., Pardigon, N., Reynes, J.M., Pettinelli, F*., et al.* (2006). Genome microevolution of chikungunya viruses causing the Indian Ocean outbreak. PLoS medicine *3*, e263.

Trkola, A., Purtscher, M., Muster, T., Ballaun, C., Buchacher, A., Sullivan, N., Srinivasan, K., Sodroski, J., Moore, J.P., and Katinger, H. (1996). Human monoclonal antibody 2G12 defines a distinctive neutralization epitope on the gp120 glycoprotein of human immunodeficiency virus type 1. J Virol *70*, 1100-1108.

Voss, J.E., Vaney, M.C., Duquerroy, S., Vonrhein, C., Girard-Blanc, C., Crublet, E., Thompson, A., Bricogne, G., and Rey, F.A. (2010). Glycoprotein organization of Chikungunya virus particles revealed by X-ray crystallography. Nature *468*, 709-712.

Walker, L.M., Huber, M., Doores, K.J., Falkowska, E., Pejchal, R., Julien, J.P., Wang, S.K., Ramos, A., Chan-Hui, P.Y., Moyle, M.*, et al.* (2011). Broad neutralization coverage of HIV by multiple highly potent antibodies. Nature *477*, 466-470.
Walker, L.M., Phogat, S.K., Chan-Hui, P.Y., Wagner, D., Phung, P., Goss, J.L., Wrin, T., Simek, M.D., Fling, S., Mitcham, J.L.*, et al.* (2009). Broad and potent neutralizing antibodies from an African donor reveal a new HIV-1 vaccine target. Science *326*, 285-289.
Yang, X., Farzan, M., Wyatt, R., and Sodroski, J. (2000). Characterization of stable, soluble trimers containing complete ectodomains of human immunodeficiency virus type 1 envelope glycoproteins. Journal of virology *74*, 5716-5725.

	IgH	IgL
NIH45-46	1.90	1.44
NIH45-46^{W}	2.40	1.35
m2	2.21	1.66
VRC01	2.41	1.54
VRC01^{W}	2.19	1.49
m66	1.59	1.47
m66^{HKK}	1.73	1.75
m66.6	1.92	1.19

Table S1. Molecular dynamics simulation of HIV-1 bNAb variants. Related to Figure 6. Values of root mean square (rms) for heavy (IgH) and light (IgL) chains are given. For the m66 antibody variants, the loop segment of residues 101-114 was not included in the rms calculation due to disorder.

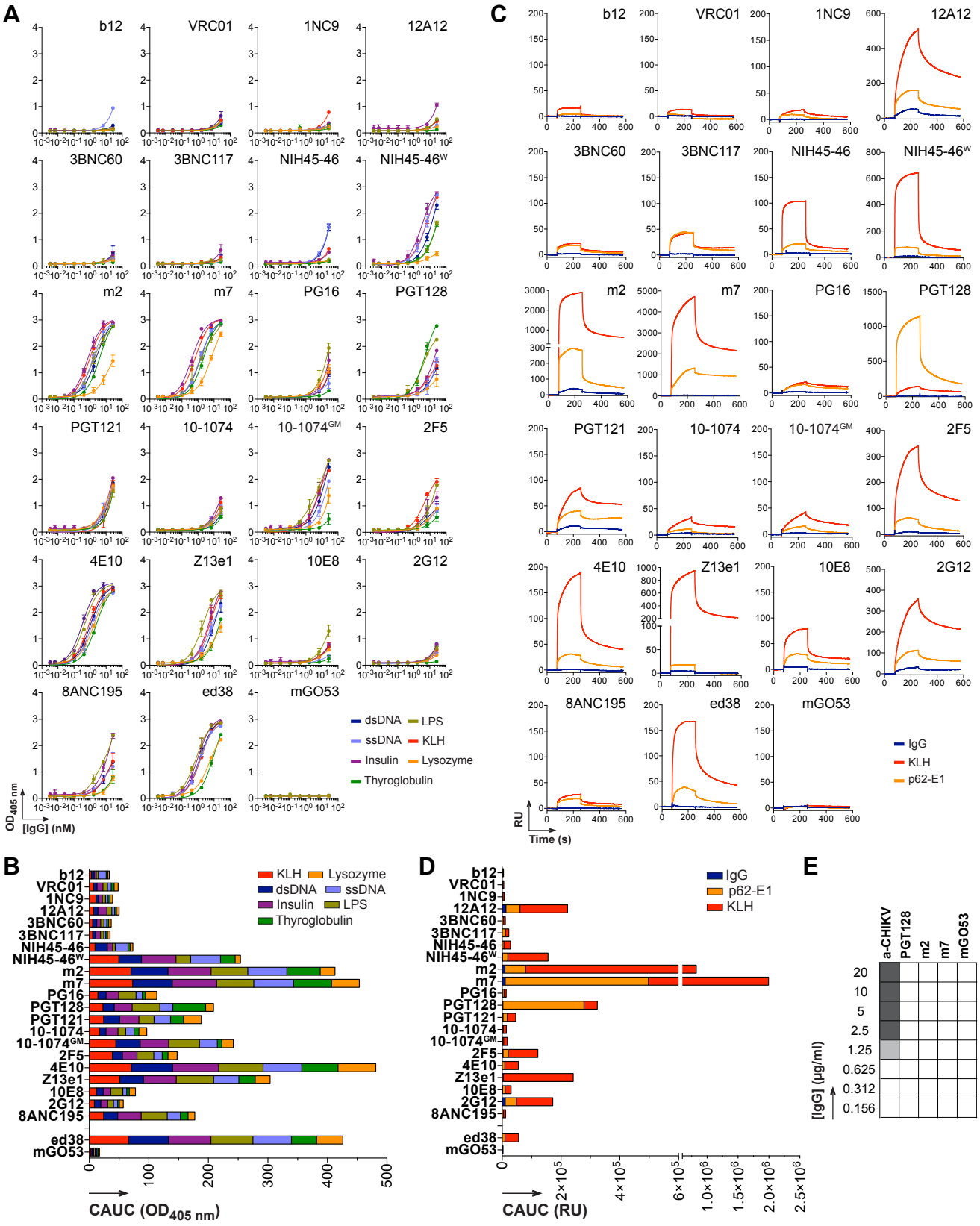

Figure S1. Polyreactivity of HIV-1 bNAbs. Related to Figure 1. (A) Polyreactivity of HIV-1 bNAbs and control antibodies were measured by ELISA against dsDNA, ssDNA, insulin, keyhole limpet hemocyanin (KLH), thyroglobulin and lysozyme. mGO53 (Wardemann et al., 2003) and ED38 (Meffre et al., 2004) are negative and positive control antibody, respectively. Error bars indicate the SEM of duplicate OD405 nm values. **(B)** Bar graph comparing the cumulative area under the curves (CAUC) for the polyreactive ELISA binding of bNAbs as measured in (A). **(C)** Surface plasmon analysis (SPR) sensorgrams show the binding overtime of IgG antibodies to human IgG1, KLH and Chikungunya envelope protein p62-E1 (Voss et al., 2010). The y axis shows the response units (RU) obtained at a given time (s, seconds) indicated on the x axis. **(D)** Bar graph comparing CAUC values for the polyreactive SPR binding of bNAbs as measured in (C). **(E)** Heat map comparing the in vitro neutralization activities of PGT128, m2, and m7 against CHIKV infection of Vero cells. Anti-CHIKV and mGO53 are positive and negative control antibodies, respectively. Neutralization activity measured in duplicate is color-coded: black, neutralization; grey, intermediate neutralization; white, no neutralization.

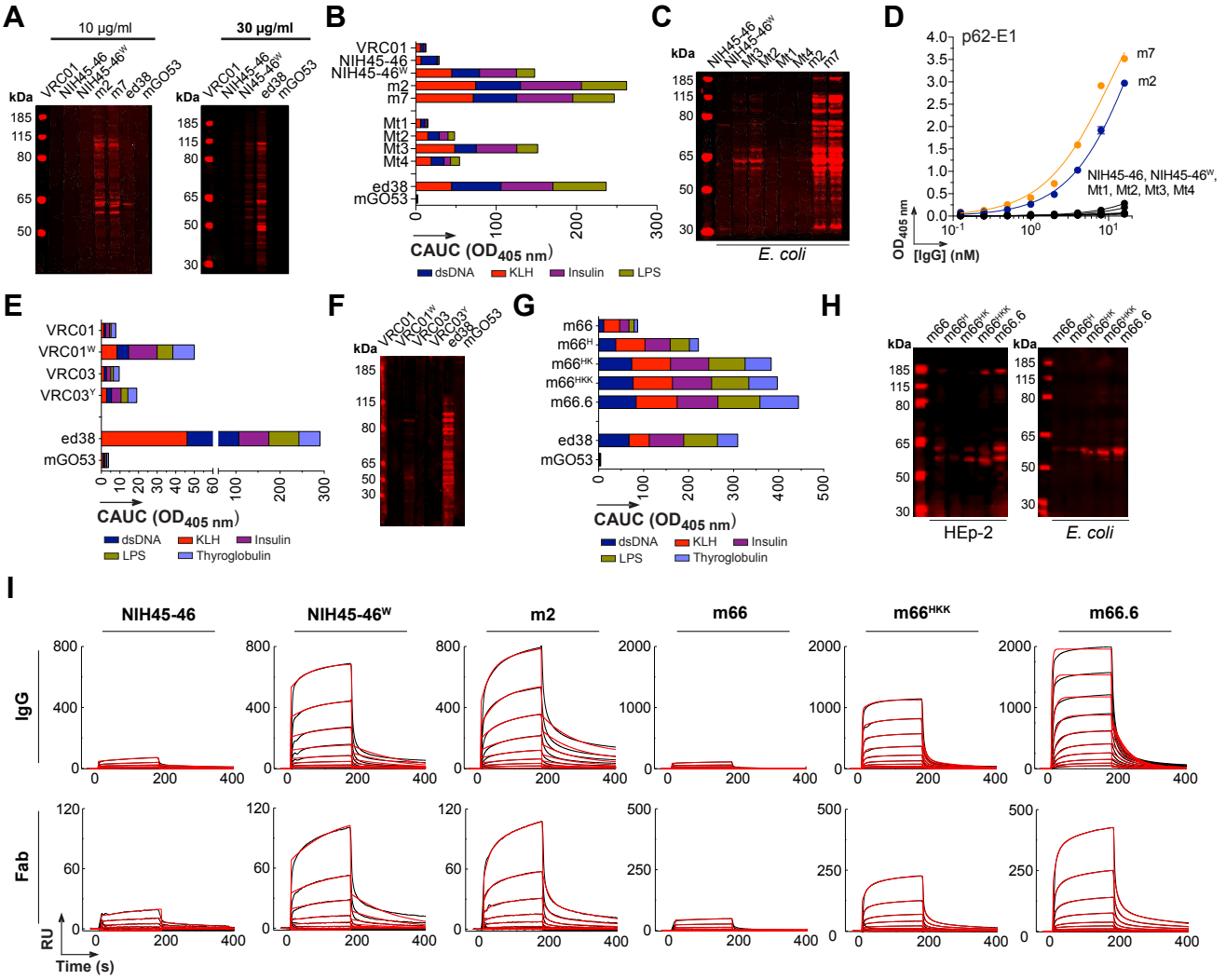

Figure S2. Polyreactive binding of HIV-1 bNAb variants. Related to Figure 2. (A) Immunoblot scans show the binding of rationally designed NIH45-46 antibody variants and controls to HEp-2 protein extract. **(B)** Bar graph comparing CAUC values for the polyreactive ELISA binding of NIH45-46 IgG variants measured in triplicate. **(C)** Representative immunoblot scans (from 2 independent experiments) show the binding of NIH45-46 mutant and control antibodies to E. coli protein extract. **(D)** ELISA graphs show the binding of NIH45-46 antibody variants and controls to Chikungunya p62-E1 glycoprotein. Error bars indicate the SEM of duplicate OD405 nm values. **(E)** Same as in (B) but for VRC01/3 and mutant IgG antibodies. **(F)** Same as in (A) but for VRC01/3 and mutant IgG antibodies (tested at 20 µg/ml). **(G)** Same as in B but for m66 and antibody variants. **(H)** Representative immunoblot scans (from 2 independent experiments) show the binding of m66, m66.6 and antibody variants to E. coli and HEp-2 protein extracts. **(I)** SPR sensorgrams comparing the binding of the selected IgG bNAbs and corresponding Fabs to KLH. The y axis shows the response units (RU) obtained at a given time (s, seconds) indicated on the x axis.

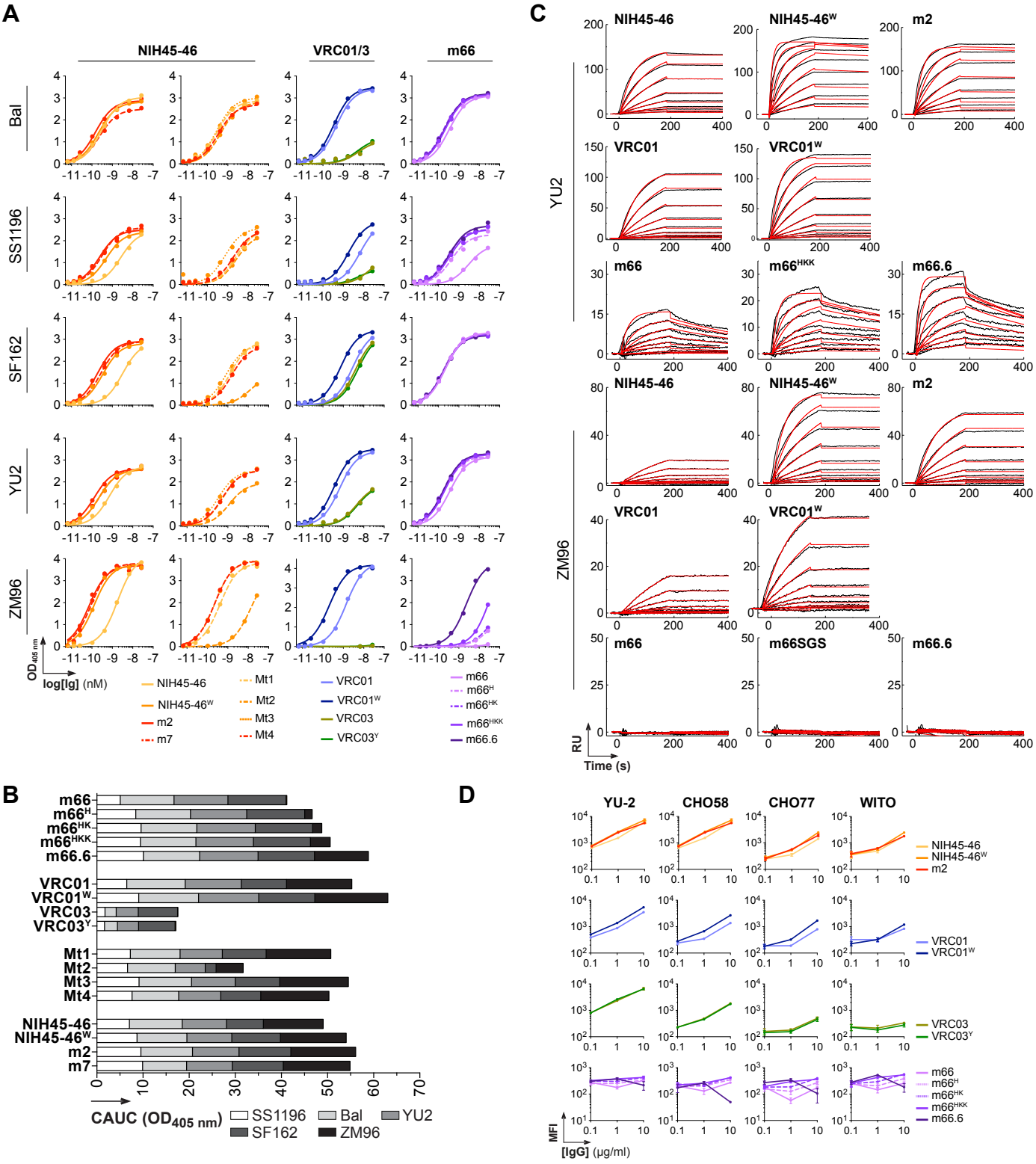

E

Virus	Clade	VRC01 IC50	VRC01 IC80	VRC01W IC50	VRC01W IC80	VRC03 IC50	VRC03 IC80	VRC03Y IC50	VRC03Y IC80
6535.3	B	5.08	21.09	0.56	4.03	1.13	8.90	1.02	5.85
YU2.DG	B	0.21	0.55	0.09	0.24	0.03	0.09	0.03	0.09
CAAN5342.A2	B	1.99	7.09	0.69	2.44	7.27	39.94	6.73	>50
THRO4156.18	B	11.32	49.99	2.56	10.04	>50	>50	>50	>50
CAP45.2.00G3	C	>50	>50	0.06	0.36	>50	>50	>50	>50
CAP210.2.00.E8	C	>50	>50	18.20	>50	>50	>50	>50	>50
Du172.17	C	>50	>50	0.17	0.91	>50	>50	>50	>50
ZM53M.PB12	C	1.56	5.85	0.51	1.86	10.42	>50	6.23	>50
3016.v5.c45	D	0.21	0.73	0.09	0.25	>50	>50	>50	>50
Q23.17	A	0.14	0.47	0.05	0.13	0.09	0.34	0.07	0.26
CNE8	CRF01_AE	0.98	3.45	0.36	1.23	42.77	>50	>50	>50
211-9	CRF02_AG	49.04	>50	1.64	8.36	>50	>50	>50	>50
MuLV	Neg. Control	>50	>50	>50	>50	>50	>50	>50	>50

Figure S3. HIV-1 Env cross-reactivity and -neutralization of polyreactive bNAb variants. Related to Figure 3. (A) ELISA graphs showing the binding of selected bNAbs to various trimeric gp140 glycoproteins. Error bars indicate the SEM of duplicate or triplicate OD405 nm values from 1-2 experiments. **(B)** Bar graph comparing CAUC values for the ELISA binding of IgG bNAbs to HIV-1 Env proteins as measured in A. **(C)** SPR sensorgrams comparing the binding of the selected IgG bNAbs to YU-2 and ZM96 gp140 glycoproteins. The y axis shows the response units (RU) obtained at a given time (s, seconds) indicated on the x axis. **(D)** Graph comparing the mean fluorescence intensity (MFI) values for binding of bNAb variants to selected viral strains exposed at the surface of infected target cells as measured by flow cytometry. Error bars indicate the SEM of triplicate MFI values from 2 independent experiments. **(E)** Table shows IC50 and IC80 values (from triplicate) for the neutralization of the selected IgG bNAbs against a panel of pseudoviruses used in TZM-bl assay. >50, 50% neutralization was not reached at 50 μg/ml. MuLV, Murine leukemia virus; Neg., negative.

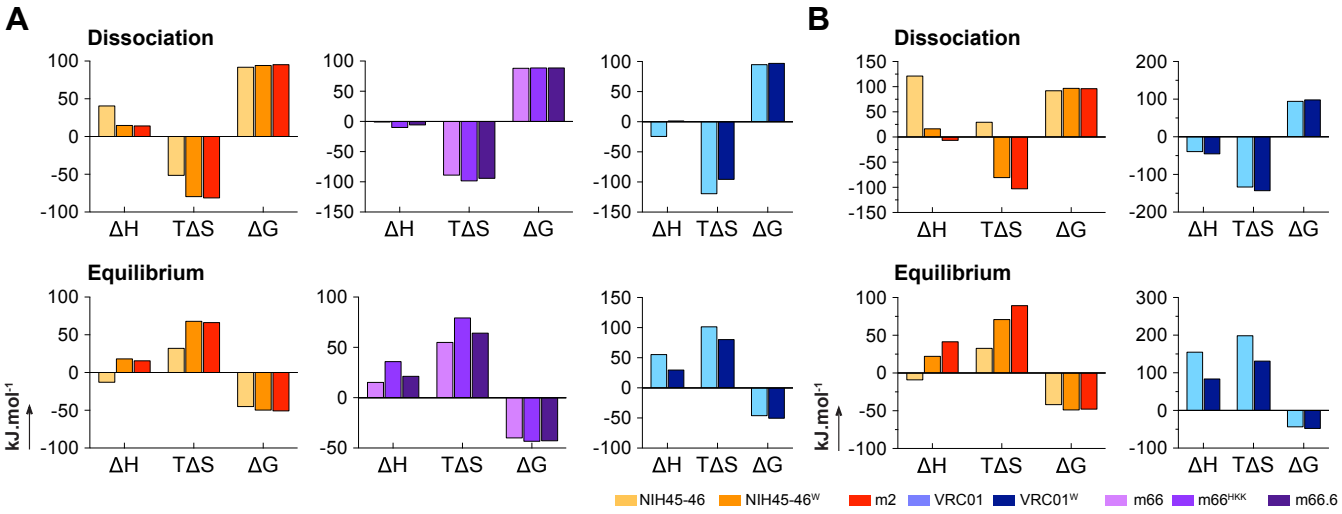

Figure S4. Binding thermodynamics of bNAb Fabs. Related to Figure 4. (A) Bar graph comparing the thermodynamic parameters for the binding of selected bNAbs to YU-2 gp140 ligands, calculated by Eyring's analyses using slopes of Arrhenius plots during the dissociation phase and at the equilibrium. **(B)** Same as in (A) but for the binding to ZM96 gp140. All thermodynamic parameters were calculated at a reference temperature of 25°C (298.7 K).

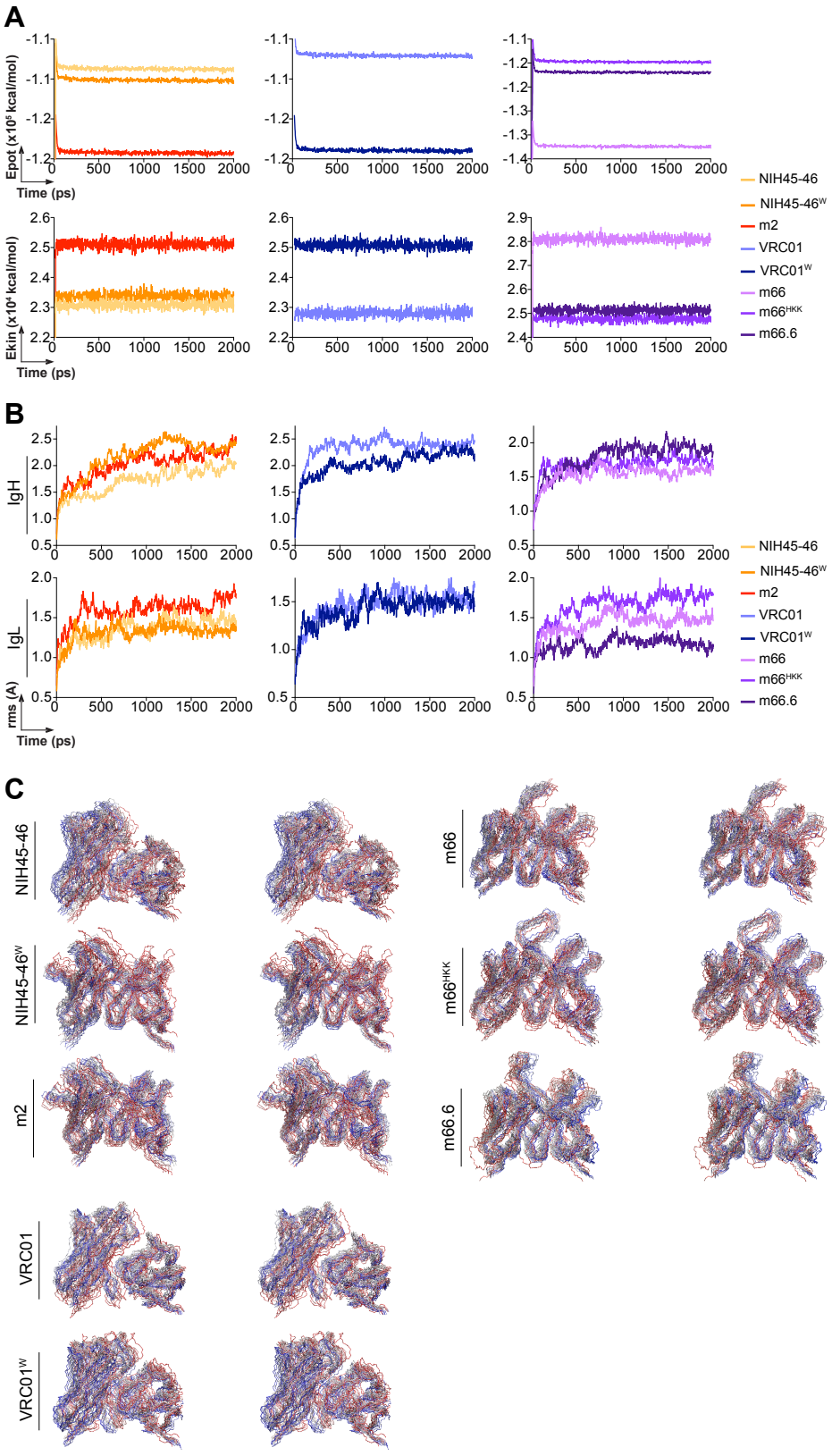

Figure S5. Molecular dynamics simulation of bNAbs' antigen binding sites. Related to Figure 6. (A) Graph comparing the total energy profile of bNAbs' antigen binding sites (ABS) overtime during the MD simulation. **(B)** Graph comparing the root-mean-square deviation (rms) of all atoms of bNAbs' ABS during the MD run. **(C)** Stereoscopic representations of the backbone atoms of bNAbs' ABS structures generated every 100 ps from the MD run. Gradient coloring of the structures represent the time points of trajectory during MD, with red and blue being the start and the end, respectively.

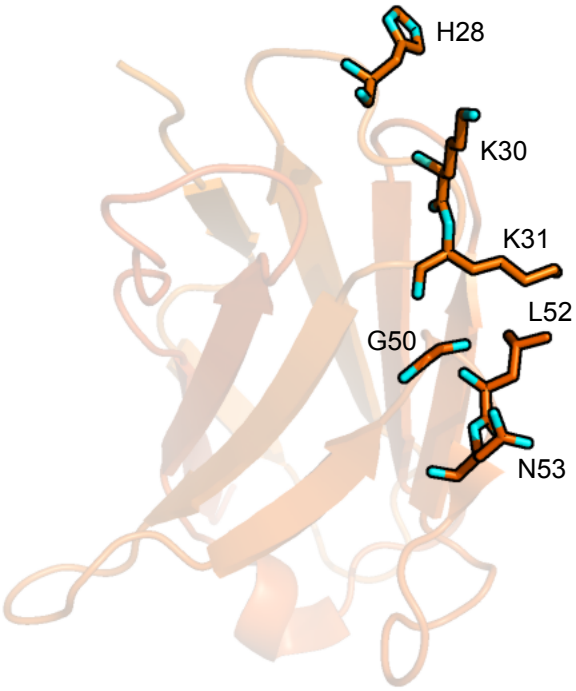

Figure S6. Structure of m66.6 IgL variable domain. Related to Figure 6.
Ribbon diagram of the crystal structure m66.6 IgL variable domain (adapted from PDB ID 4NRZ (Ofek et al., 2014)) highlighting residues H28K30K31 of the CDRH1 loop and G50L52N53 of the CDRH2 loop.